Paleoceanography and Paleoclimatology

RESEARCH ARTICLE
10.1029/2022PA004501

A brGDGT-Based Reconstruction of Terrestrial Temperature From the Maritime Continent Spanning the Last Glacial Maximum

M. C. Parish[1], X. Du[1,2], S. Bijaksana[3], and J. M. Russell[1]

[1]Department of Earth, Environmental, & Planetary Sciences, Brown University, Providence, RI, USA, [2]Institute at Brown for Environment and Society, Brown University, Providence, RI, USA, [3]Global Geophysics Group, Faculty of Mining and Petroleum Engineering, Institut Teknologi Bandung, Bandung, Indonesia

Key Points:

- We produced a 60,000-year long temperature reconstruction based on branched glycerol dialkyl glycerol tetraethers (brGDGTs) measured in a lake sediment core from Sulawesi, Indonesia
- We separate the influence of lake chemistry changes from temperature changes on the brGDGT records to develop the temperature record
- The timing of warming in our record occurs after the onset of the deglacial increase in CO_2, which suggests CO_2 forced deglacial warming

Supporting Information:

Supporting Information may be found in the online version of this article.

Correspondence to:

M. C. Parish,
meredith_parish@brown.edu

Citation:

Parish, M. C., Du, X., Bijaksana, S., & Russell, J. M. (2023). A brGDGT-based reconstruction of terrestrial temperature from the maritime continent spanning the last glacial maximum. *Paleoceanography and Paleoclimatology*, *38*, e2022PA004501. https://doi.org/10.1029/2022PA004501

Received 29 JUN 2022
Accepted 31 JAN 2023

Author Contributions:

Conceptualization: M. C. Parish, S. Bijaksana, J. M. Russell
Data curation: X. Du, S. Bijaksana, J. M. Russell
Formal analysis: M. C. Parish
Funding acquisition: S. Bijaksana, J. M. Russell
Methodology: M. C. Parish, S. Bijaksana, J. M. Russell
Project Administration: S. Bijaksana, J. M. Russell
Resources: X. Du, S. Bijaksana, J. M. Russell
Supervision: S. Bijaksana, J. M. Russell
Visualization: M. C. Parish
Writing – original draft: M. C. Parish

Abstract The tropics exert enormous influence on global climate. Despite the importance of tropical regions, the terrestrial temperature history in the Indo-Pacific Warm Pool (IPWP) region during the last deglaciation is poorly constrained. Although numerous sea surface temperature (SST) reconstructions provide estimates of SST warming from the Last Glacial Maximum to the Holocene, the timing of the onset of deglacial warming varies between records and inhibits determining the forcings driving deglacial warming in the IPWP. We present a 60,000-year long temperature reconstruction based on branched glycerol dialkyl glycerol tetraethers (brGDGTs) in a sediment core from Lake Towuti, located in Sulawesi, Indonesia. BrGDGTs are bacterial membrane-spanning lipids that, globally, become more methylated with decreasing temperature and more cyclized with decreasing pH. Although changes in temperature are the dominant control on brGDGTs in regional and global calibrations, we find that the cyclization of the brGDGTs is a major mode of variation at Lake Towuti that records important changes in the lacustrine biogeochemical environment. We separate the influence of lake chemistry changes from temperature changes on the brGDGT records, and develop a temperature record spanning the last 60,000 years. The timing of the deglacial warming in our record occurs after the onset of the deglacial increase in CO_2 concentrations, which suggests rising greenhouse gas concentrations and the associated radiative forcing may have forced deglacial warming in the IPWP. Peaks in temperature around 55 and 34 ka indicate that Northern Hemisphere summer insolation may also influence land surface temperature in the IPWP region.

Plain Language Summary The tropics play an important role controlling global climate because they export heat to higher latitudes. Even though the tropics are important, we do not actually know the primary control on tropical temperature. We created a 60,000-year long record of temperature because this length of record spans large changes in the proposed controls on tropical climate (greenhouse gas concentrations and incoming solar radiation). We created a temperature record from a lake sediment core from Lake Towuti in Indonesia. Since sediment gradually accumulated in the bottom of Lake Towuti for over 60,000 years, we took one sample from the lake sediment core every 6 cm to give us one sample every 500 years. We measured different types of molecules that compose the outer protective barrier (membrane) of bacteria cells. The molecules in the membrane are different in cold than hot environments. We measured the abundance of hot-adapted and cold-adapted membrane lipids to determine the temperature in the past. The timing of warming after the last glacial period occurs after the onset of the increase in CO_2 concentrations, which suggests rising greenhouse gas concentrations and the associated radiative forcing may be the dominant control on temperature over the past 60,000 years.

1. Introduction

Three major zones of deep atmospheric convection energize the Earth's moisture and energy budgets: tropical Africa, Amazonia, and the Indo-Pacific Warm Pool (IPWP; Figure 1; Chiang, 2009). The IPWP is by far the largest of these, where sea surface temperatures (SSTs) above 28°C extend over an area of more than 30 million km^2, and the region exerts enormous influence on global climate through its interactions with the Walker Circulation, the Austral-Asian monsoons, and the Intertropical Convergence Zone (ITCZ; Chiang, 2009; De Deckker, 2016). Regionally, precipitation is intimately linked to surface temperature over the IPWP with high SSTs generating deep atmospheric convection and some of the highest precipitation rates on Earth (De Deckker, 2016; Figure 1).

Writing – review & editing: X. Du, S. Bijaksana, J. M. Russell

Reconstructing a continuous record of terrestrial temperature spanning the past 60 thousand years (kyr) in the IPWP will provide insight into how changing boundary conditions (e.g., insolation and CO_2) from the Last Glacial Maximum (LGM) to modern (Shakun et al., 2012) influenced regional climate, how IPWP climate change will interact with global climate processes in the future, and how increasing anthropogenic CO_2 emissions will impact Indonesia, the fourth most populous country on Earth (Current Population, 2022).

The dominant forcing of deglacial warming in the IPWP is debated, due in large part to a wide range of estimates for the timing of the onset of deglacial warming in the region. The onset of warming indicated in SST records varies from 20.4 to 17.9 ka among existing SST records from the IPWP (Bolliet et al., 2011; Fan et al., 2018; Gibbons et al., 2014; Holbourn et al., 2011; Jian et al., 2020; Levi et al., 2007; Mohtadi et al., 2014; Rosenthal et al., 2003; Schröder et al., 2018; Setiawan et al., 2015; Steinke et al., 2006; Stott et al., 2007; Wang et al., 2018; Xu et al., 2008), spanning the onset of deglacial changes in northern hemisphere insolation and the global onset of increasing CO_2 concentrations after the LGM. The wide range of ages for the onset of deglacial warming has led to a variety of hypotheses for the forcings that control regional temperature, from teleconnections to the northern high latitudes (Stott et al., 2007) to a dominant control by atmospheric CO_2 concentrations (Shakun et al., 2012). Furthermore, to date, temperature reconstructions from this region are almost entirely from marine settings, complicating assessment of terrestrial temperature change. Terrestrial temperature is of particular importance in the tropics because convection there is centered over land masses (Chiang, 2009).

To uncover the forcings of terrestrial temperature in the IPWP, we reconstructed temperatures using sediment cores from Lake Towuti, Indonesia, spanning the past 60 kyr. This interval includes the last deglaciation, the most recent time interval when global warming was accompanied by rising greenhouse gas concentrations. We produced a terrestrial temperature reconstruction based on the fractional abundances of branched glycerol dialkyl glycerol tetraethers (brGDGTs), membrane-spanning lipids whose degree of methylation increases with decreasing temperatures to maintain membrane fluidity (Naafs et al., 2021). The degree of methylation of brGDGTs in lacustrine sediment samples is highly correlated with mean annual air temperature (MAAT) in tropical environments (Russell et al., 2018). Although these global relationships are well-established, Lake Towuti is a relatively unique, ferruginous environment and its microbial communities are likely not well-represented in existing surface sediments used in brGDGT calibrations (Martínez-Sosa et al., 2021; Raberg et al., 2021; Russell et al., 2018). Indeed, the IPWP region is not represented well in existing brGDGT calibrations and regional temperatures can exceed the limits of currently available temperature calibrations. We therefore evaluate brGDGTs in this environment to assess the applicability of existing calibrations and the environmental controls on brGDGT abundances through the 60-kyr record. We then reconstruct terrestrial temperature from Lake Towuti in Indonesia to evaluate the influences of atmospheric CO_2 concentrations and insolation as primary drivers of IPWP terrestrial temperature from the LGM to modern. As the first quantitative terrestrial temperature reconstruction in the IPWP region, our record provides additional constraints on the driving forcing of IPWP climate.

2. Study Site, Materials, and Methods

2.1. Study Site

Lake Towuti is located near the equator (2.75°S, 121.5°E) in central Sulawesi, Indonesia at an elevation of 318 m (Figure 1). Sulawesi is a 174,600 km^2 island in the center of the IPWP. Lake Towuti has a surface area of 560 km^2 and a maximum water depth of 203 m. Modern lake surface temperatures of Lake Towuti range seasonally from 29° to 31°C, with cooler temperatures in austral winter and spring and the warmest temperatures in austral fall (Russell et al., 2020). The water column mixes seasonally to ∼100 m depth but a permanent thermocline at 100 m depth separates oxic waters at the surface from hypoxic to anoxic waters below (Costa et al., 2015). The pH is ∼7.8 and the lake is ultraoligotrophic. The lake is one of a handful of ferruginous (high iron-low sulfate) systems that exist on Earth today due to its location within the East Sulawesi ophiolite (Crowe et al., 2008; Vuillemin et al., 2016). This setting establishes an uncommon biogeochemical environment within the lake, and the extremely low primary productivity at Lake Towuti has been attributed to low nutrient delivery from surrounding soil and phosphate removal related to high iron concentrations (Crowe et al., 2008; Russell et al., 2020).

The samples analyzed in this study were subsampled from a piston core (IDLE-TOW10-9B) extracted from the center of Lake Towuti's northern basin (Russell et al., 2014, 2020). We analyzed 115 samples, spanning the past 60,000 years for an average sampling resolution of ∼500 years, with a minimum sampling resolution of 82 years

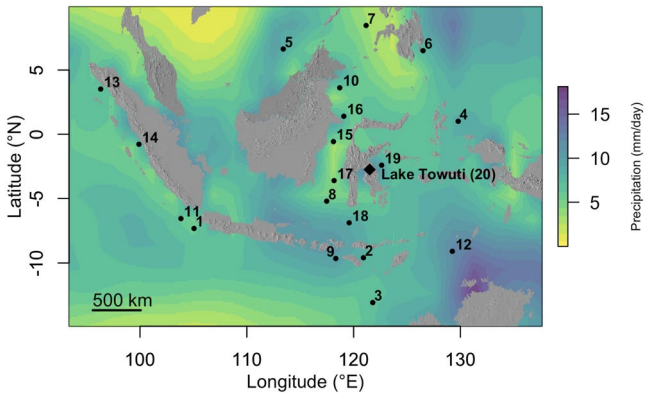

Figure 1. Lake Towuti (2.75°S, 121.5°E) is located in central Sulawesi, Indonesia, at an elevation of 318 m, shown with a diamond. The map also shows nearby SST records that span the last deglaciation, numbered as follows: 1. GeoB10043 (Setiawan et al., 2015), 2. GeoB10069 (Gibbons et al., 2014), 3. MD01-2378 (Xu et al., 2008), 4. MD01-2386 (Jian et al., 2020), 5. MD01-2390 (Steinke et al., 2006), 6. MD06-3067 (Bolliet et al., 2011), 7. MD97-2141 (Rosenthal et al., 2003), 8. MD98-2161 (Fan et al., 2018), 9. MD98-2165 (Levi et al., 2007), 10. MD98-2178 (Fan et al., 2018), 11. SO139-74KL (Wang et al., 2018), 12. SO185-18460 (Holbourn et al., 2011), 13. SO189-119KL (Mohtadi et al., 2014), 14. SO189-39KL (Mohtadi et al., 2014), 15. SO217-18519 (Schröder et al., 2018), 16. SO217-18522 (Schröder et al., 2018), 17. SO217-18526 (Schröder et al., 2018), 18. SO217-18540 (Schröder et al., 2018), 19. TGS-931 (Schröder et al., 2018), and 20. Lake Towuti (this study). Mean annual precipitation per day is shown based on 1991–2021 precipitation reanalysis data (Kalnay et al., 1996). Precipitation and the digital elevation models are plotted using the "raster" package in *R* (Hijmans et al., 2022).

and maximum sampling resolution of 3575 years. The mean sampling resolution during the last deglaciation (22 to 11.6 ka) is 430 years. There are 23 radiocarbon dates in the top 43-kyr of sediment, which we calibrated to Intcal20 and used to estimate the age of every centimeter of sediment with Bacon in *R* (Blaauw & Christen, 2011).

2.2. Lipid Extraction and Analysis

Lipids were extracted from sediment using a DIONEX Accelerated Solvent Extractor using dichloromethane:methanol (9:1). The lipid extract was divided into neutral and acid fractions using dichloromethane:isopropanol (2:1) and ethyl ether:acetic acid (96:4) over an aminopropyl silica gel column for previous analyses (Konecky et al., 2016). Silica gel columns were used to separate lipids within the neutral fraction, using hexane to isolate n-alkanes, dichloromethane to isolate ketones, and methanol to isolate the remaining hydroxides. We used Al_2O_3 columns to further separate the hydroxide fraction into apolar and polar fractions with the eluents hexane:dichloromethane (9:1) and dichloromethane:methanol (1:1). The polar fraction was filtered through 0.45 μm PTFE filter in hexane: isopropanol (99:1).

We analyzed the polar fractions using atmospheric pressure chemical ionization/high-performance liquid chromatography mass spectrometry (APCI/HPLC-MS) with a bridged ethylsiloxane/silica hybrid (BEH) hydrophilic interaction chromatography (HILIC) 1.7 μm (2.1 mm inner diameter × 150 mm length) column using selective ion monitoring mode, targeting molecules at m/z 1,050, 1,048, 1,046, 1,036, 1,034, 1,032, 1,022, 1,020, 1,018, 1,292, 1,296, 1,298, 1,300, and 1,302 (Hopmans et al., 2016). Ten percent of samples were run in duplicate to assess the precision of the measurements. We manually integrated peak areas of both 5-methyl isomers (Ia, Ib, Ic, IIa, IIb, IIc, IIIa, IIIb, IIIc) and 6-methyl isomers (IIa', IIb', IIc', IIIa', IIIb', IIIc') to quantify the relative abundances of the brGDGTs in each sample.

2.3. Analyses of the Fractional Abundances of GDGTs

Empirical studies, theory, and molecular simulations indicate that the number of methyl branches in brGDGTs increases at decreasing temperatures to maintain cell membrane fluidity (Loomis et al., 2012, 2014; Martínez-Sosa et al., 2021; Naafs et al., 2021; Raberg et al., 2021; Russell et al., 2018; Tierney & Russell, 2009; Tierney et al., 2010). However, water chemistry, microbial community composition, and other factors may also affect brGDGT relative abundances (Loomis et al., 2014; Martínez-Sosa et al., 2021; Wu et al., 2021). We used principal component analysis (PCA) to evaluate the primary modes of variability in brGDGT abundances in downcore samples from Lake Towuti. We performed a PCA analysis based on the correlation matrix of the fractional abundances of the major brGDGTs in the Lake Towuti record (Ia, Ib, Ic, IIa, IIa', IIb, IIb', IIc', IIIa'), using the princomp() function in the "vegan" package in *R* (Oksanen et al., 2020). The nine major brGDGTs each comprised more than two percent of the total abundance of brGDGTs in at least one sample over the past 60,000 years (Ia, Ib, Ic, IIa, IIa', IIb, IIb', IIc', IIIa').

Many index-based calibrations and multiple linear regression models exist to translate the signals reflected in changing brGDGT assemblages into paleoenvironmental and paleoclimatic parameters (e.g., temperature). Index-based calibrations are based on our theoretical and empirical understanding that brGDGTs with fewer methyl branches increase with increasing temperature, and brGDGTs with fewer cyclopentane rings are more abundant in environments with a higher pH (Weijers et al., 2007). MBT'_{5ME} (Equation 1) is the ratio of brGDGTs with four methyl branches or substituted cyclopentane moieties relative to the total abundance of brGDGTs with 4–6 methyl branches or substituted rings (De Jonge et al., 2013; Russell et al., 2018) and it increases with increasing temperature. To calculate MAAT from MBT'_{5ME}, we used the calibration from Russell et al. (2018) (Equation 2).

$$MBT'_{5ME} = \frac{(Ia + Ib + Ic)}{(Ia + Ib + Ic + IIa + IIb + IIc + IIIa)} \quad (1)$$

$$MAAT = -1.21 + 32.42 \times MBT'_{5ME} \quad (2)$$

In addition to index-based calibrations, there are various multiple linear regression methods based on the best statistical fits of brGDGT fractional abundances to temperature. These methods generally confirm the basic principles inherent to index-based calibrations (i.e., the degree of methylation increases with decreasing temperature), but may include a distinct set of brGDGTs potentially due to influences of multiple correlated environmental parameters on brGDGT abundances (Loomis et al., 2014). Among these calibrations, we calculated the temperature of the months above freezing (MAF) using the stepwise forward selection/backwards elimination (SFS/SBE) equation published in the supplement of Raberg et al. (2021) (Equation 3). We used the calibration recommended for samples with limited quantities of IIIb and IIIc because these brGDGTs comprised less than 1% of the brGDGTs in all samples from Lake Towuti. The equation is based on the fractional abundances of IIa and IIIa, where fIIa is the fraction of IIa relative to Ia, IIa, and IIIa; and fIIIa is the fraction of IIIa relative to Ia, IIa, and IIIa.

$$MAF = 26.56 - 34.67\left(fIIa^2_{meth}\right) + 29.4\left(fIIIa^2_{meth}\right) - 49.43(fIIIa_{meth}) \quad (3)$$

We calculated MAAT using the SFS/SBE equation (Equation 4) based on the fractional abundances of the major brGDGTs in 65 lakes from tropical east Africa (Loomis et al., 2012, 2014; Russell et al., 2018). The SFS/SBE equation shows MAAT decreases with increasing penta- and hexamethylated brGDGTs (e.g., IIa, IIb, IIb', and IIIa), and MAAT increases with increasing tetramethylated brGDGTs (e.g., Ib).

$$MAAT = 23.04 - 30.09\,(IIIa) - 45.31(IIb) - 46.56(IIb') - 22.65(IIa) + 72.85(Ib) \quad (4)$$

We also calculated a new SFS/SBE-based MAAT equation with all global lacustrine samples presented in Martinez-Sosa et al. (2021) and a new SFS/SBE equation based on all samples in the global database that have less than 50% hexamethylated brGDGTs. As hexamethylated brGDGTs are most abundant in cool environments, this restricts the calibration to warmer climates where calibration to MAAT may be more appropriate. We focus on MAAT rather than the mean temperature of MAF (Martínez-Sosa et al., 2021; Raberg et al., 2021) in our choice of calibrations, though MAAT and MAF are equivalent in the tropics due to the lack of seasonality. These SFS/SBE equations are presented in the results section.

The cyclization of branched tetraethers (CBT) indices (Equations 5 and 6) were calculated using brGDGTs with varying degrees of cyclization to evaluate variations in lake pH (De Jonge et al., 2014; Sinninghe Damsté et al., 2012; Tierney et al., 2010; Weijers et al., 2007). We use the CBT_{5ME} index from De Jonge et al. (2014):

$$CBT_{5ME} = -\log((Ib + IIb)/(Ia + IIa)) \quad (5)$$

We also use the CBT' from De Jonge et al. (2014):

$$CBT' = -\log\left(\left(Ic + IIa' + IIb' + IIc' + IIIa' + IIIb' + IIIc'\right)/(Ia + IIa + IIIa)\right) \quad (6)$$

We evaluated the branched and isoprenoidal tretraether (BIT) index (Equation 7; Hopmans et al., 2004; Tierney et al., 2010), which reflects the amount of branched GDGTs (Ia, IIa, IIIa) relative to the amount of branched and isoprenoidal GDGTs (isoGDGTs) as indicated by crenarchaeol (IV).

$$BIT = \frac{([Ia] + [IIa] + [IIIa])}{([Ia] + [IIa] + [IIIa] + [IV])} \quad (7)$$

In addition to analyses of brGDGTs, we analyzed the relative abundances of isoGDGTs, which are produced by Thaumarchaeota. Previous work has shown that the degree of cyclization of isoGDGTs increases with increasing temperature in both marine and lacustrine settings, and developed the TEX_{86} index (Equation 8), the ratio of isoprenoidal GDGTs with 2–3 rings and the regio-isomer of crenarchaeol (IV') relative to the number of isoGDGTs with 1–3 rings and IV', to quantify this relationship. The number of rings in isoGDGTs in the TEX_{86} index increases with increasing temperature (Powers et al., 2010; Schouten et al., 2002).

$$TEX_{86} = \frac{\left([GDGT2] + [GDGT3] + [IV']\right)}{([GDGT1] + [GDGT2] + [GDGT3] + [IV'])} \quad (8)$$

However, the relative abundances of isoGDGTs may also be influenced by changes in the relative inputs of terrestrial and aquatic isoGDGTs, as well as other microbial community changes. Comparison between the BIT index

and the TEX_{86} index allows us to test whether TEX_{86} reflects changes in soil runoff amount (Sinninghe Damsté et al., 2012) or other environmental factors (Baxter et al., 2021).

2.4. Changepoint Analysis

We determined the timing of deglacial warming in our temperature record using the EnvCpt package in *R* to find significant changepoints in the trend (slope) in the data (Killick et al., 2021). The changepoints were determined by calculating a stepwise linear function that minimizes the total residual error. We selected the changepoint detected between 22 and 14 ka as the timing of deglacial warming. Additionally, we calculated the changepoints of atmospheric CO_2 and nearby SST records to compare with the timing of deglacial changes to the Lake Towuti temperature record using identical methods.

3. Results

3.1. Abundances of Tetra-, Penta-, and Hexa-Methylated brGDGTs Relative to Calibration Data Sets

The fractional abundance of brGDGTs from Lake Towuti are dominated by tetramethylated brGDGTs, with greater than 50% brGDGTs with four methyl groups in every sample (Figures 2 and 3). After tetramethylated

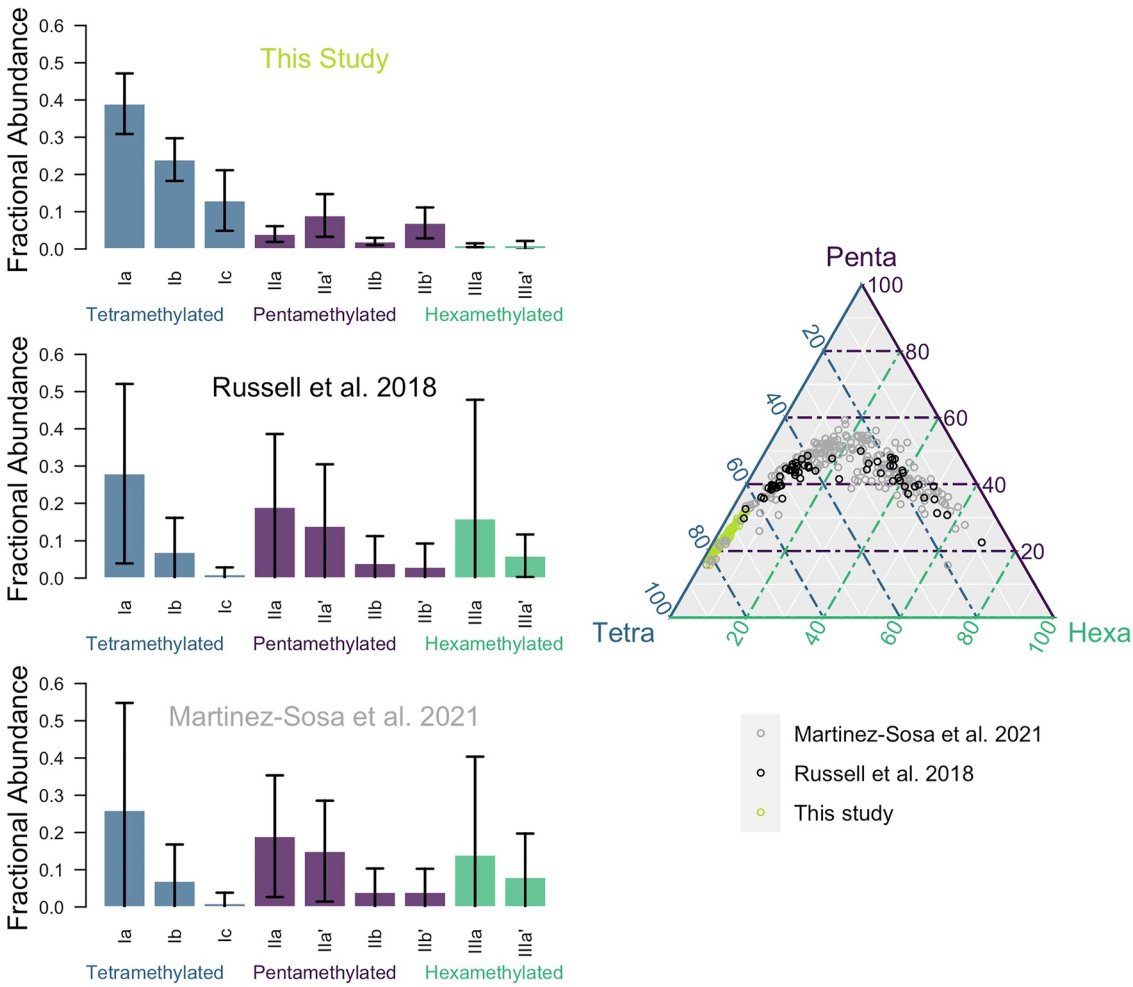

Figure 2. The average fractional abundances of the individual brGDGTs in all samples from the past 60,000 years from Lake Towuti, plotted as the mean ±2 standard deviations. A ternary diagram of the fractional abundances of summed tetramethylated, pentamethylated, and hexamethylated brGDGTs in all samples from Lake Towuti relative to modern samples from East African lakes (Russell et al., 2018) and global lakes (Martínez-Sosa et al., 2021). The ternary diagram is plotted using the "ggtern" package in *R* (Hamilton, 2022).

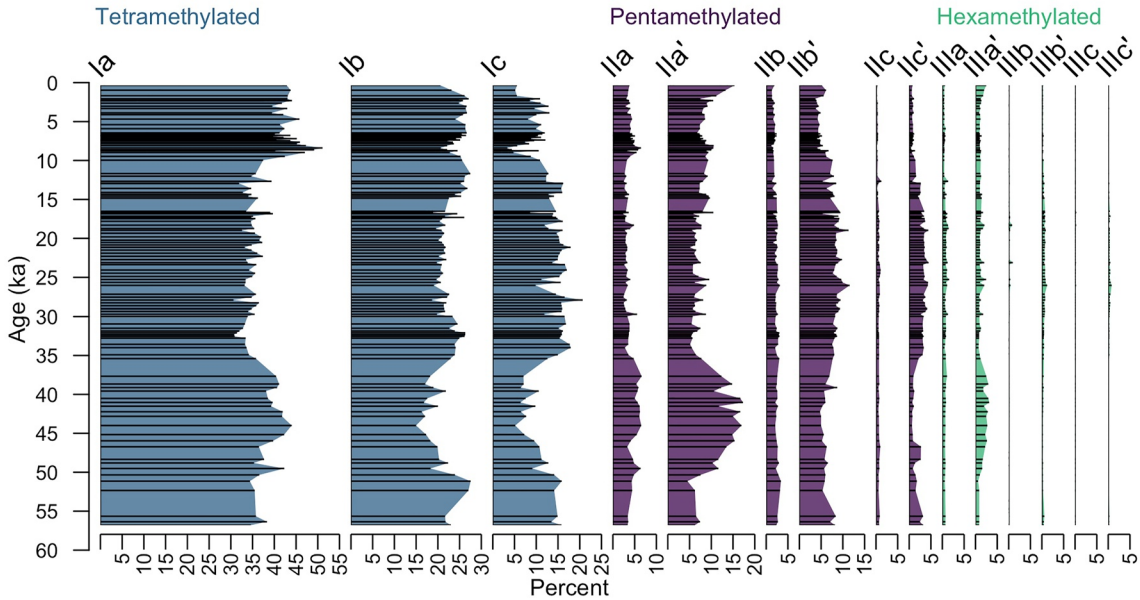

Figure 3. Percent of total tetramethylated (blue), pentamethylated (purple), and hexamethylated (green) brGDGTs in downcore samples from Lake Towuti. The fractional abundance data is plotted using the strat.plot() function in the "Rioja" package in *R* (Juggins, 2022).

brGDGTs, pentamethylated brGDGTs are the most abundant brGDGTs in Lake Towuti samples. Hexamethylated brGDGTs make up less than 10% of the total brGDGTs in every sample. Tetramethylated brGDGTs are much more abundant in almost all samples from Lake Towuti than in samples from tropical southeast Africa (Figure 2; Russell et al., 2018) and globally (Figure 2; Martínez-Sosa et al., 2021), and although Lake Towuti samples are in a compositional field that might be expected of a lacustrine setting, they are primarily outside the range of samples in existing calibration datasets (Figure 2). Hexamethylated brGDGTs have more methyl branches than tetra- and pentamethylated brGDGTs, and are found in higher abundance in colder environments. Therefore, the low abundance of hexamethylated brGDGTs and high abundance of tetramethylated brGDGTs is consistent with the high mean annual temperatures observed at Lake Towuti relative to the environments in existing global calibrations.

BrGDGT Ia, containing four methyl groups and zero cyclopentane rings, is the most abundant brGDGT throughout the past 60,000 years (Figure 3). The highest abundances of Ia occur around 45 ka and the lowest abundance between 35 and 10 ka. Ib and Ic are the second and third most abundant brGDGTs, and show the opposite trends as Ia, exhibiting the lowest values of the record at 45 and 10 ka with sustained high abundances from 35 to 10 ka. IIa shows a similar pattern as Ia but is less abundant than each of the tetramethylated brGDGTs. IIb is less variable over the past 60,000 compared to the other brGDGTs due to low abundance. IIb' varies similarly to Ic with the highest abundances at 60 ka and between 30 and 10 ka. IIc' has less than 5% abundance throughout the record with the lowest abundances from 50 to 35 ka and from 15 ka to present. IIc, IIIa, IIIb, IIIb', IIIc, and IIIc' have the lowest abundances (less than 2%) in every samples during the past 60,000 years. IIIa' comprises over 2% of the total abundance of brGDGTs in some samples during the past 60,000 years with the highest abundances between 55 and 40 ka.

3.2. PCA of Fractional Abundances of brGDGTs

A PCA reveals two principal components that explain a total of 80% of the variance in the fractional abundances of brGDGTs. PC1 explains 54% of the variance and PC2 explains 26% of the variance (Figure 4c). All of the brGDGTs without cyclopentane moieties (Ia, IIa, IIa', and IIIa') have positive loadings on PC1, all of the brGDGTs with one cyclopentane moiety (Ib, IIb, and IIb') have negative loadings on PC1, and brGDGTs with two cyclopentane moieties (Ic and IIc') have even greater magnitude negative loadings on PC1. The distribution of these brGDGTs along PC1 indicates that PC1 reflects the cyclization of brGDGTs (Figure 4c). PC1 has the

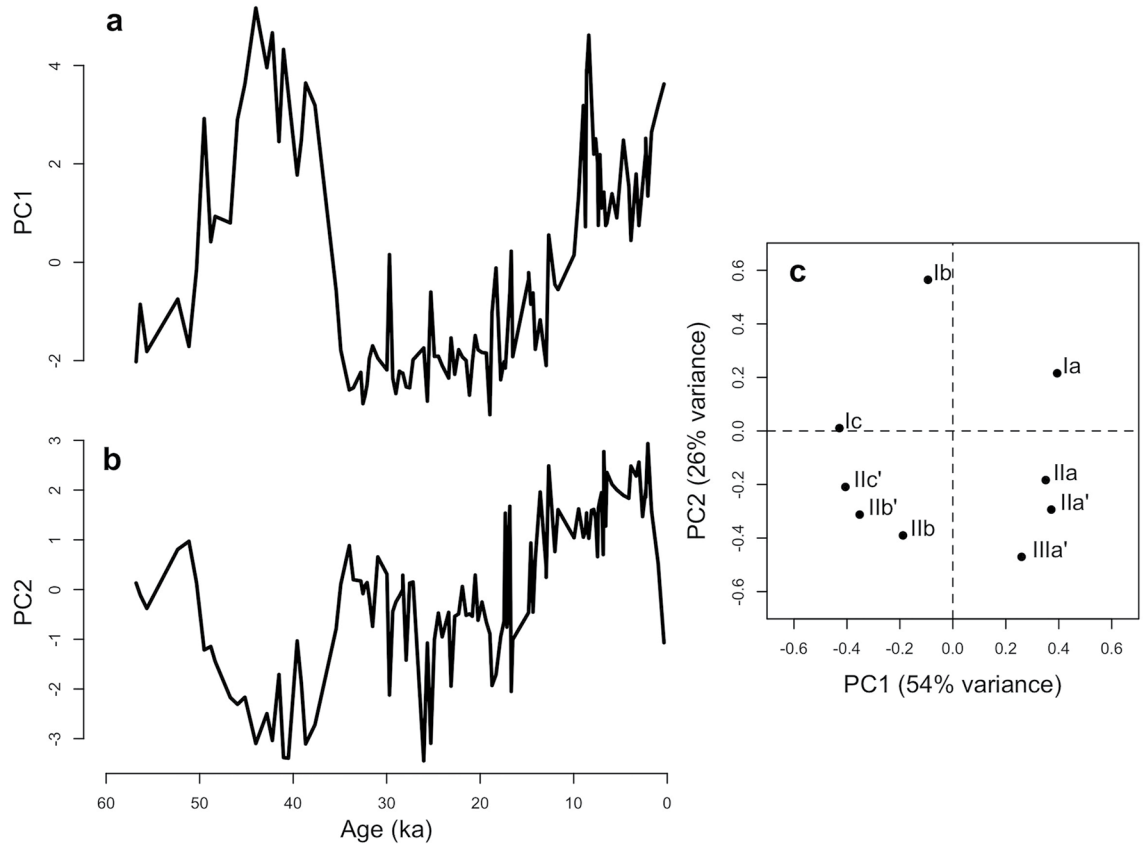

Figure 4. Principal component analysis based on the correlation matrix of the fractional abundances of brGDGTs which comprised more than two percent of the total abundance of brGDGTs in at least one sample over the past 60,000 years (Ia, Ib, Ic, IIa, IIa', IIb, IIb', IIc', IIIa'), made using the princomp() function from the "vegan" *R* package to calculate the principal components based on the correlation matrix of the fractional abundances of the major brGDGTs. (a) PC1 scores of every sample, (b) PC2 scores of every sample, and (c) the loadings of the major brGDGTs on PC1 and PC2.

highest component scores at 45 and 10 ka and lowest scores from 60 to 50 ka and between 35 and 15 ka (Figure 4a).

Tetramethylated brGDGTs (Ia, Ib, and Ic) have a positive or zero loading on PC2 (Figure 4c). Pentamethylated brGDGTs (IIa, IIa', IIb, IIb', and IIc') have negative loadings on PC2. The only hexamethylated brGDGT with greater than 2% abundance in one sample from the record (IIIa') has the greatest negative loadings on PC2, indicating that PC2 reflects the methylation of brGDGTs throughout the Lake Towuti record. PC2 has the lowest component scores between 50 and 40 ka and at 27 ka, before increasing into the Holocene (Figure 4b).

3.3. Methylation and Temperature

The MBT'$_{5ME}$-index varies between 0.86 and 0.94 throughout the entire record. These high values reflect the high proportion of tetramethylated brGDGTs in all samples from Lake Towuti and therefore predict high temperatures over the past 60,000 years (Figure S1a in Supporting Information S1). The lowest MBT'$_{5ME}$-values occur between 50 and 40 ka when the proportion of tetramethylated brGDGTs, driven by Ib and Ic, are at their lowest throughout the record. MAAT calculated from the MBT'$_{5ME}$-index is positively correlated with PC2 (Figure 5; $R = 0.79$, all reported correlation coefficients have a p-value less than 0.01), presumably reflecting the importance of Ia and Ib to both PC2 and the MBT'$_{5ME}$-index. Using the Russell et al. (2018) MBT'$_{5ME}$ temperature calibration results in the lowest temperature of the record (26.6°C) at 38 ka and the highest temperature of the record (29.7°C) at 13 ka (Figure S1a in Supporting Information S1).

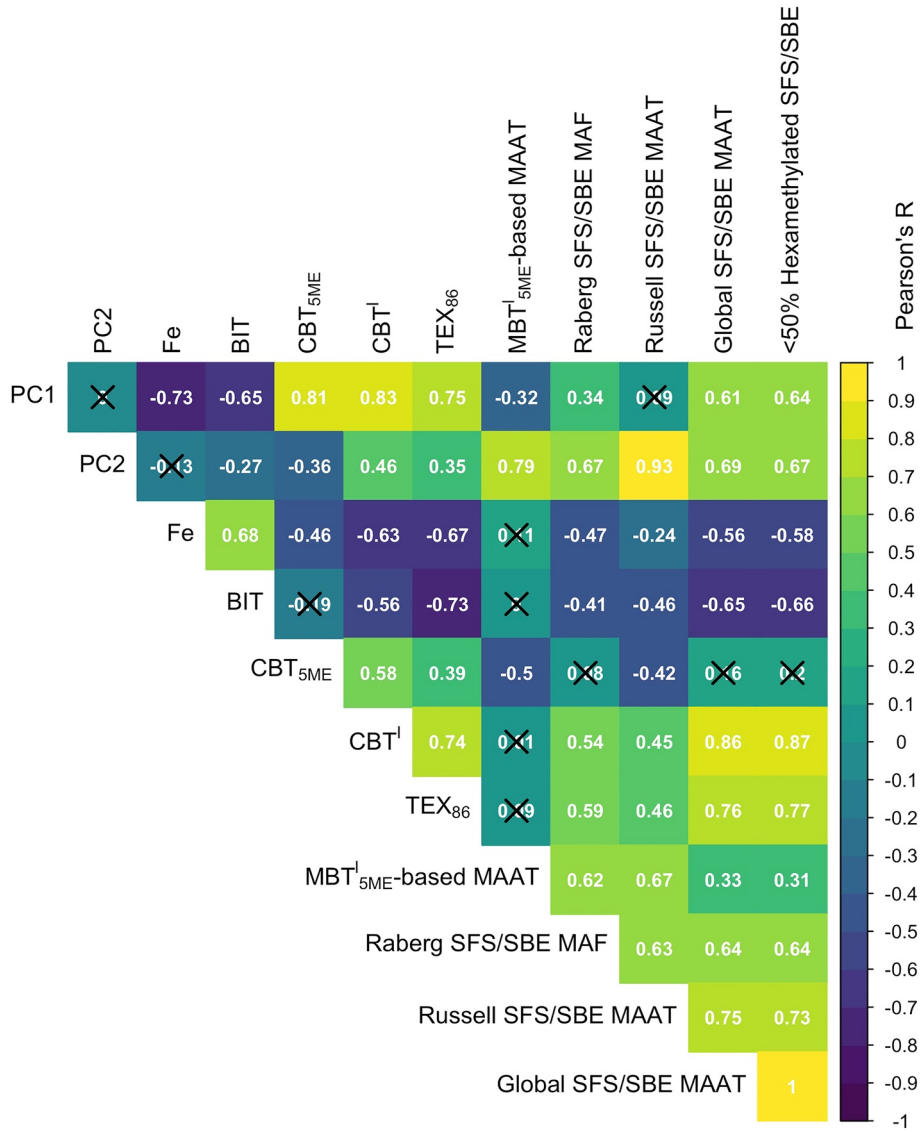

Figure 5. Correlation matrix showing Pearson's *R* between PC1 and PC2; Iron measured in the Lake Towuti sediment core (Costa et al., 2015); indices based on the fractional abundances of GDGTs in the Lake Towuti record, including: BIT, CBT_{5ME}, TEX_{86}, and MBT'_{5ME}-based MAAT (Equation 2; Russell et al., 2018); SFS/SBE-based reconstructions using published equations from global (Equation 3; Raberg et al., 2021) and East African lake sediment samples (Equation 4; Russell et al., 2018); and new SFS/SBE equations presented in this study from all global lake sediment samples published in Martinez-Sosa et al. (2021) (Equation 9) and samples with less than 50% hexamethylated brGDGTs, representing hotter environments (Equation 10). All reported Pearson correlation coefficients are significant at 99% confidence level ($p < 0.01$, $n = 115$), except correlation coefficients with a black x that indicates a p-value greater than 0.01. The correlation matrix is plotted using the "corrplot" package in *R* (Wei et al., 2021).

The Raberg et al. (2021) MAF SFS/SBE produces temperatures that vary between 24.2°C and 26.0°C, with the lowest temperatures of the record occurring between 30 and 20 ka (Figure S1c in Supporting Information S1). The MAF reconstruction is moderately correlated with PC2 (Figure 5; $R = 0.67$). The MAF SFS/SBE only includes fIIa and fIIIa. IIIa comprises less than two percent of all samples from Lake Towuti and is therefore not included in the PCA analysis and IIa only has a weak negative loading on PC2. Therefore, it is not surprising that the correlation is lower than the MBT'_{5ME}-MAAT and Russell SFS/SBE MAAT correlation with PC2 (Figure 5).

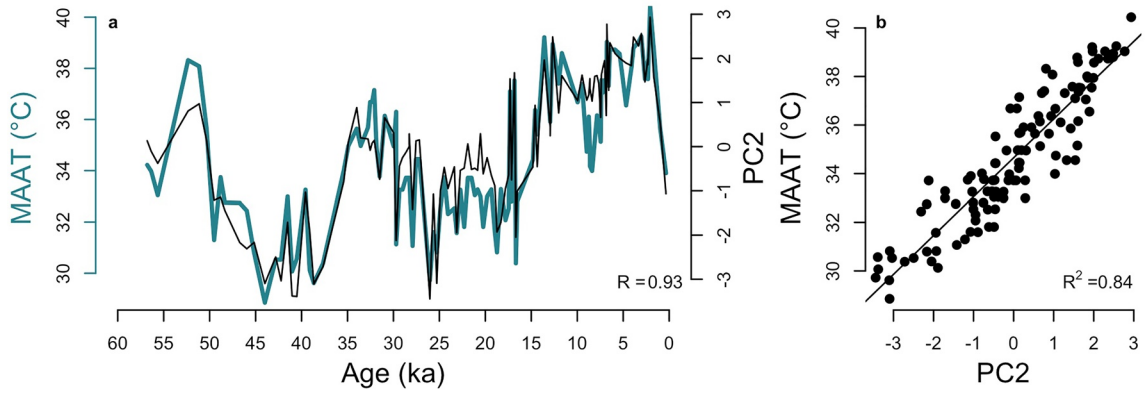

Figure 6. (a) Mean annual air temperature (MAAT) as reconstructed by the SFS/SBE equation based on the fractional abundances of the major brGDGTs in 65 lakes from tropical east Africa published in Russell et al. (2018) (teal). PC2 from the principal component analysis shown in Figure 4 (black). The Pearson correlation coefficient between MAAT and PC2 is 0.93, also shown in Figure 5. (b) Linear regression between MAAT and PC2, and the associated R^2.

The new global SFS/SBE regression calculated using all global lacustrine samples included in Martinez-Sosa et al. (2021) and identical methods as Russell et al. (2018) is (Equation 9):

$$\mathrm{MAAT} = 6.04 + 91.93\,(\mathrm{Ib}) + 22.78(\mathrm{Ia}) - 27.59(\mathrm{IIa}) - 25.16\left(\mathrm{IIIa}'\right) - 72.52(\mathrm{Ic}) \quad (9)$$

The global SFS/SBE regression using the same method but only including "warm lake" samples with less than 50% hexamethylated brGDGTs is (Equation 10):

$$\mathrm{MAAT} = 10.63 + 84.23\,(\mathrm{Ib}) + 18.32(\mathrm{Ia}) - 34.71(\mathrm{IIa}) - 41.72\left(\mathrm{IIIa}'\right) - 78.76(\mathrm{Ic}) \quad (10)$$

Stepwise forward selection regressions thus select the same compounds (Ia, Ib, Ic, IIa, and IIIa') using global or "warm lake" datasets but differ from the brGDGTs used in SFS/SBE regression based on tropical East African samples alone (Ib, IIb, IIb', and IIIa; Equation 4; Russell et al., 2018). Both the global and less than 50% hexamethylated SFS/SBE reconstructions result in similar temperature records over the past 60,000 years (Figures S1e and S1g in Supporting Information S1), and are positively correlated with PC2 ($R = 0.69$ and $R = 0.67$, respectively; Figure 5). Ia and Ib, which are included in the SFS/SBE equations (Equations 9 and 10), have strong positive loadings on PC2 and IIa, and IIIa' have negative loadings on PC2. Ic, which is also included in the SFS/SBE equations, has a near zero loading on PC2, potentially explaining the relatively weak correlations.

The tropical East African SFS/SBE model produces a temperature reconstruction that indicates relatively high temperatures ca. 55 ka, the lowest temperatures in the record between 50 and 37 ka (Figure 6a), a cool LGM that extends from ~27 to 17 ka and warming from the LGM into the Holocene. The temperature reconstruction is highly correlated with PC2 ($R = 0.93$, shown in Figure 5; $R^2 = 0.84$, shown in Figure 6b). The brGDGTs included in the tropical African SFS/SBE (Ib, IIb, IIb', and IIIa) all have strong loadings on PC2 with the exception of IIIa, which comprises less than 2% of all samples from the Lake Towuti record. Assuming that the tropical East African SFS/SBE calibration reflects changing temperature, PC2 reflects changes in temperature and therefore that temperature explains approximately 26% of the total variance in fractional abundances of all major brGDGTs.

The Raberg et al. (2021) calibration is strongly dependent on the fractional abundance of IIIa (Raberg et al., 2021), which has very low abundance in most of the Lake Towuti samples. The magnitude of LGM to modern temperature change in Lake Towuti produced by this calibration is less than two degrees, which is inconsistent with nearby SST reconstructions (Rosenthal et al., 2003; Schröder et al., 2018; Stott et al., 2007). We therefore do not use the Raberg et al. (2021) calibration in further analyses. We also do not use $\mathrm{MBT'}_{5\mathrm{ME}}$-based calibration (Russell et al., 2018) to infer temperature. The PCA of the down-core fractional abundances of brGDGTs from Lake Towuti reveals that Ic, which is included in the $\mathrm{MBT'}_{5\mathrm{ME}}$-index, varies with the principal component that may reflect lake pH (PC1) rather than lake temperature (PC2). Ic is also included in the global and "warm lake" SFS/SBE equations. The tropical East African SFS/SBE temperature reconstruction (Russell et al., 2018), in contrast, is based on brGDGTs that principally load on PC2, mitigating these effects. In the following analyses and discussion, we use the tropical African SFS/SBE reconstruction because it has the strongest correlation with PC2 and thus appears to capture the influence of temperature on the brGDGTs at this site.

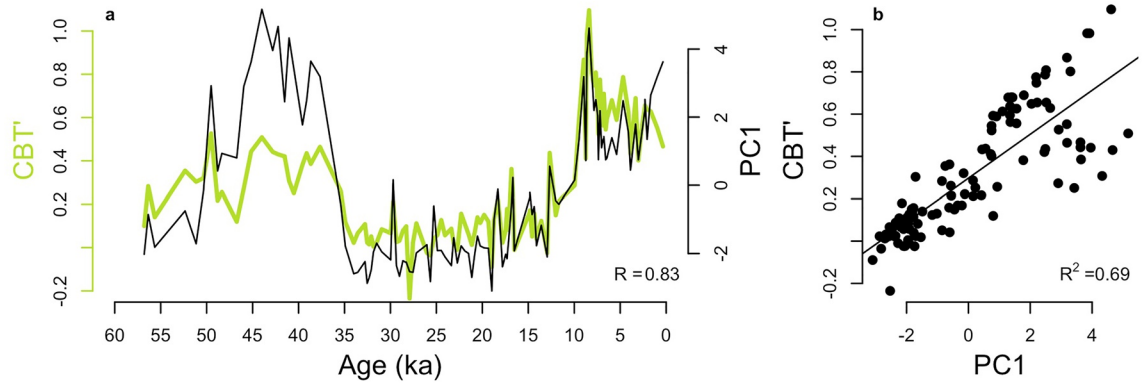

Figure 7. (a) The CBT' index based on the fractional abundances of brGDGTs in the Lake Towuti record (green) and PC1 from the principal component analysis shown in Figure 4 (black). The Pearson correlation coefficient is 0.83, shown in Figure 5. (b) Linear regression between the CBT' and PC1, and the associated R^2.

3.4. Cyclization, pH, and Isoprenoidal GDGTs

The CBT_{5ME} index indicates an interval of abundant cyclized brGDGTs at ~45 ka, a sustained period of low CBT_{5ME} values from 35 to 11 ka, and an abrupt increase to the highest values of the record around ~10 ka (Figure S2g in Supporting Information S1). CBT_{5ME} closely tracks and is highly correlated with PC1 ($R = 0.81$, Figure 5), confirming that PC1 primarily reflects variations in the cyclization of brGDGTs. Ia and IIa are included in the denominator of the CBT_{5ME} index and have strong loadings on PC1, whereas Ib and IIb are included in the numerator of the CBT_{5ME} index and have negative loadings on PC1. In prior calibration studies CBT_{5ME} has been shown to depend on pH and conductivity (Martínez-Sosa et al., 2021; Raberg et al., 2021). Although this is not always the case in lacustrine sediment calibrations (e.g., Russell et al., 2018), previous studies in Lake Towuti and the surrounding catchment demonstrated that CBT_{5ME} values increased from soils, to river sediments, to lake sediments associated with decreasing pH in these environments (Tierney & Russell, 2009). We infer that the strong correlation of CBT_{5ME} with PC1 indicates the majority of variation in the fractional abundances of the brGDGTs that load on PC1 depend on the pH, and potentially conductivity, of Lake Towuti. Using CBT_{5ME} to reconstruct pH using the soil-based calibration from De Jonge et al. (2014) results in a pH of ~7 from 35 to 11 ka, a sharp drop in pH around 10 ka, before hovering around a pH of ~6.8 during most of the Holocene (Figure S3 in Supporting Information S1). The CBT' index behaves similarly to the CBT_{5ME} index, however the peak in CBT_{5ME} at 45 ka is much less pronounced in the CBT' record (Figure S2 in Supporting Information S1). CBT' is more highly correlated with PC1 ($R = 0.83$, shown in Figure 5, $R^2 = 0.69$, shown in Figure 7b) than CBT_{5ME}. The lake CBT'-base calibration from Russell et al. (2018) indicates lower pH values from 35 to 11 ka than from 10 ka, which indicates that Lake Towuti was more acidic at the LGM. More acidic lake water at the LGM contradicts existing data, which indicate more basic lake water at the LGM (Costa et al., 2015). However, CBT' was weakly correlated with pH in the East African lakes studied by Russell et al. (2018).

Both the BIT index and the TEX_{86} index are significantly correlated with PC1 ($R = -0.65$ and $R = 0.75$, respectively; Figure 5). The correlation of both BIT and TEX_{86} with PC1 indicates that both indices primarily reflect the cyclization of brGDGTs and likely the lake chemistry. BIT and TEX_{86} are also negatively correlated with each other ($R = -0.73$), indicating that TEX_{86} may not reflect temperature and is influenced by the abundance of crenarchaeol (Baxter et al., 2021; Tierney et al., 2010). These correlations imply that BIT is impacted by lake chemistry, terrigenous sediment fluxes, or other environmental parameters that influence GDGT sources to the sediment (Sinninghe Damsté et al., 2012).

3.5. Timing of Temperature Change

Changepoint analysis of the temperature reconstruction from Lake Towuti based on the East African lake SFS/SBE indicates that deglacial warming begins at 17.5 ka (Figure 8), over 1,000 years after the onset of deglacial increase in CO_2 at 18.7 ka as indicated by identical changepoint detection methods applied to the West Antarctic Ice Sheet (WAIS) Divide CO_2 record (Marcott et al., 2014). Application of the changepoint analysis to nearby SST records indicates deglacial warming starts at a wide range of times. The SST record off the coast of Sumatra

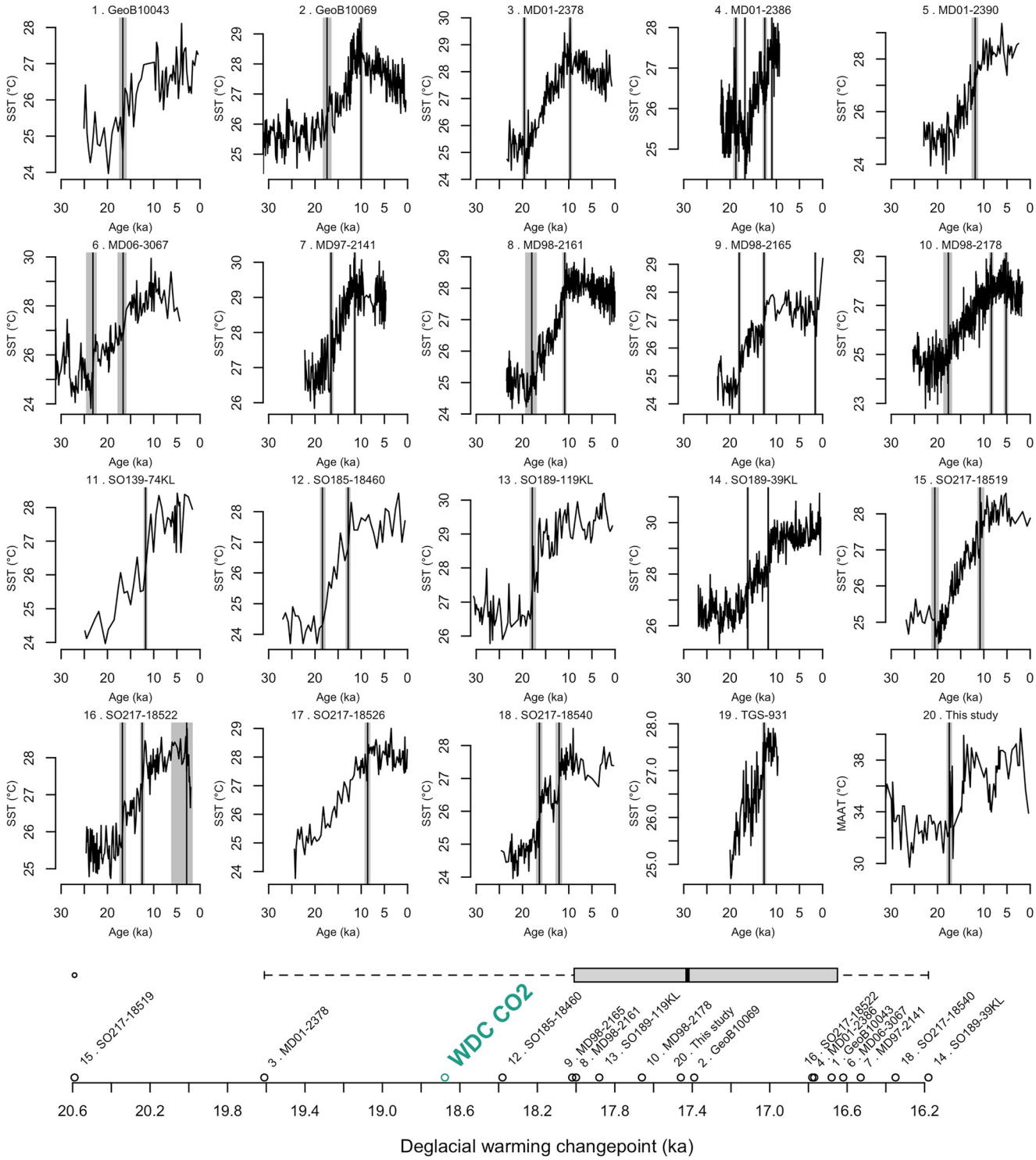

Figure 8.

has the latest onset of deglacial warming at 16.2 ka (SO189-39KL; Mohtadi et al., 2014), whereas the earliest deglacial warming occurs at 20.6 ka in the Makassar Strait (SO217-18519; Schröder et al., 2018). The timing of deglacial warming indicated in the Lake Towuti records lies exactly on the median timing of warming of all the SST records included in our analysis.

4. Discussion

4.1. Variations in brGDGTs in Sediments From Lake Towuti

Previous work investigating brGDGTs in Lake Towuti, inflowing rivers, and surrounding soils has demonstrated in-situ production of brGDGTs in Lake Towuti (Tierney & Russell, 2009), suggesting changes in the fractional abundances of brGDGTs depend on environmental variables in the lake rather than surrounding soil. Temperature explains the majority of variance in the fractional abundances of brGDGTs in global lacustrine samples (Martínez-Sosa et al., 2021) and in tropical East Africa (Russell et al., 2018). Globally, pH explains only 12% of the variance in the abundances of brGDGTs (Martínez-Sosa et al., 2021) and in tropical East Africa lake water pH does not cause significant variation (Russell et al., 2018). In contrast to brGDGTs in these global datasets, we observe that cyclization, which is most dependent on the pH of the lake water in which the brGDGTs were produced (Martínez-Sosa et al., 2021; Raberg et al., 2021), explains the majority (54%) of the variance in the fractional abundances of brGDGTs in the Lake Towuti record (Figure 4c). Changes in methylation of the brGDGTs is the second mode of variation, explaining 26% of the variance in the brGDGT assemblages (Figure 4c). PC1 is strongly correlated with the CBT_{5ME} index and PC2 correlates with the temperature record reconstructed using the East African SFS/SBE from Russell et al. (2018).

Prior sedimentological studies of Lake Towuti support the inference that changes in PC1 through time reflect changes in lake water chemistry. Lake Towuti experienced very large changes in sediment composition during the LGM that reflect increased mixing, oxygenation, and pH that resulted in substantially higher oxidized metal and carbonate mineral inputs to the sediment, among other shifts (Costa et al., 2015; Russell et al., 2014, 2020). During the LGM, decreased temperatures and increased aridity led to lake surface cooling, increased lake mixing, and thereby oxygenation of the lake water column. This resulted in increased burial of reactive iron (Russell et al., 2020). At the same time, authigenic carbonate in the form of siderite increased during this interval, potentially reflecting increased pH and the burial of reactive iron in the surface sediments (Russell et al., 2020). Reconstructing pH with a soil calibration (De Jonge et al., 2014) indicates higher pH values at the LGM than modern. The pH values were ∼7.0 at the LGM, whereas the most modern reconstructed value was 6.6 (Figure S3 in Supporting Information S1). It should be noted that the most modern reconstructed pH value is well below the measured modern pH (7.8); however, the trend in pH values reconstructed from the cyclization index are consistent with previous climatic inferences. These biogeochemical changes were used to infer a more prolonged dry season at the LGM, which could cause increased evaporation and longwave heat loss that increased lake mixing, increase lake water pH, and increased Fe burial (Costa et al., 2015).

Iron measured in Lake Towuti's sediment is negatively correlated with PC1 ($R = -0.73$; Figure 5; Costa et al., 2015), and authigenic carbonate content of the sediment rises during the interval of high Fe. High Fe and carbonate mineral concentrations are consistent with the higher pH values inferred from CBT_{5ME} values (Costa et al., 2015; Russell et al., 2020). Field and experimental studies have shown that brGDGT assemblages depend on dissolved oxygen content and the pH of lake water (Martínez-Sosa & Tierney, 2019; Stefanescu et al., 2021; Tierney et al., 2012; Yao et al., 2020). Although it remains difficult to quantify changes in these variables through time, our results show that they can have substantial impacts on brGDGT abundances in tropical lake settings.

The changes in cyclization of brGDGTs recorded by PC1 and CBT' are consistent with elevated pH values during the LGM (Figure 7a), but it is unclear why these biogeochemical changes in the lake and shifts in cyclization dominate the variation in brGDGTs in Lake Towuti, in contrast to globally distributed lakes. Ferruginous lakes are uncommon on Earth today, and our study could suggest that the microbes that produce brGDGTs in these systems have different sensitivities to pH and temperature than in other tropical lakes.

Figure 8. IPWP SST records, numbered as follows: 1. GeoB10043 (Setiawan et al., 2015), 2. GeoB10069 (Gibbons et al., 2014), 3. MD01-2378 (Xu et al., 2008), 4. MD01-2386 (Jian et al., 2020), 5. MD01-2390 (Steinke et al., 2006), 6. MD06-3067 (Bolliet et al., 2011), 7. MD97-2141 (Rosenthal et al., 2003), 8. MD98-2161 (Fan et al., 2018), 9. MD98-2165 (Levi et al., 2007), 10. MD98-2178 (Fan et al., 2018), 11. SO139-74KL (no deglacial changepoint detected; Wang et al., 2018), 12. SO185-18460 (Holbourn et al., 2011), 13. SO189-119KL (Mohtadi et al., 2014), 14. SO189-39KL (Mohtadi et al., 2014), 15. SO217-18519 (Schröder et al., 2018), 16. SO217-18522 (Schröder et al., 2018), 17. SO217-18526 (no deglacial changepoint detected; Schröder et al., 2018), 18. SO217-18540 (Schröder et al., 2018), 19. TGS-931 (no deglacial changepoint detected; Schröder et al., 2018), and our MAAT reconstruction, 20. Lake Towuti (this study). The vertical lines indicate the timing of all the changepoints detected using the "EnvCpt" package in *R* (Killick et al., 2021), and the gray shading around the vertical lines shows the age uncertainty from the record. The boxplot shows the median, minimum, maximum, and interquartile range of all the SST deglacial changepoints and the changepoint detected in the Lake Towuti record. The timing of the deglacial changepoint detected using identical methods in the WAIS Divide ice core (WDC) CO_2 record (Marcott et al., 2014) is plotted in teal.

Principal component analysis reveals the orthogonal behavior of cyclization and methylation of the fractional abundances of the brGDGTs (Figure 4). Changes in methylation of brGDGTs represented by PC2 explain 26% of the variance in the fractional abundances of brGDGTs over the past 60,000 years. PC2 and the East African SFS reconstruction are highly correlated, and PC2 is orthogonal to PC1, giving us confidence in our ability to fully separate the influences of chemical changes in the water of Lake Towuti from the changes in temperature captured by the degree of methylation. Lake Towuti has mostly tetramethylated brGDGTs throughout the past 60,000 years, indicating that the lake experienced higher temperatures than the surface samples included in the tropical African surface sample calibration (Russell et al., 2018). The highest MAAT in the tropical African data set is 26.8°C, which is more than 3°C colder than the modern MAAT at Lake Towuti. Because Lake Towuti's modern MAAT is outside the range of the tropical East African SFS/SBE calibration we apply, we hesitate to make inferences based on the absolute values of the reconstructed temperatures. Indeed, the most modern reconstructed temperature value in the Lake Towuti record is ~34°C at 0.347 ka, which is three degrees warmer than the warm season recorded in measured lake surface temperature at Lake Towuti, again suggesting the absolute reconstructed values are inaccurate. Therefore, we do not interpret the reconstructed values as actual temperature, and instead focus on the timing and structure of the Lake Towuti MAAT record.

We use the East African SFS/SBE equation to reconstruct MAAT; however, the assemblage of brGDGTs is likely more highly correlated with lake water temperature, not air temperature. We are unable to determine whether the reconstructed temperature reflects bottom water temperature or surface water temperature. As in many tropical lakes, there is a weak temperature gradient between the surface and bottom water, with 28.4°–30.5°C surface water and 28.0°C bottom water in modern measurements (Costa et al., 2015).

4.2. Comparison to Regional LGM Temperature Records

The Lake Towuti record indicates a terrestrial temperature change from the LGM to the Holocene of 3.6°C. Although we hesitate to trust the absolute value of the reconstructed temperatures, the record may still capture the amplitude of the changes in temperature with time assuming the brGDGT-MAAT relationship is linear. Indeed, 3.6°C is within the range of deglacial warming inferred from regional palynological records, which estimate the LGM was 2°–4°C cooler than modern. At this time, lowland rainforest decreased, grassland expanded, and high-elevation plant taxa shifted downslope (Reeves et al., 2013). Another nearby pollen record from South Sulawesi was used to infer a 2.5°C temperature change from the LGM to modern (Hope, 2001), though the chronology of this record is highly uncertain. The magnitude of temperature change indicated in our temperature reconstruction is also consistent with SST records from the region. Nearby SST reconstructions from the IPWP indicate 2°–4°C of deglacial warming (Rosenthal et al., 2003; Schröder et al., 2018; Stott et al., 2007). Because of the higher heat capacity of the ocean relative to the continent, the magnitude of terrestrial temperature change is expected to be greater and more variable than changes in SSTs (Clement et al., 2004).

Changepoint analysis of Lake Towuti temperatures indicates deglacial warming began at 17.5 ± 0.33 ka. Atmospheric CO_2 concentrations and their associated radiative forcing began increasing at 18.7 ka (Figure 8; Marcott et al., 2014; Schilt et al., 2010). Warming in Lake Towuti thus began ~1 kyr after the onset of the deglacial increase in CO_2 concentrations, though this lag could narrow (or widen) given the 0.33 kyr uncertainty of the Lake Towuti age model at 17.5 ka. The timing of the onset of deglacial warming thus considerably lags changes in global forcings, such as CO_2, and occurs well in advance of more regional climate forcings, such as Sunda Shelf inundation. The lag in deglacial warming in the Lake Towuti record behind the deglacial increase in CO_2 points to greenhouse gas forcing as the primary driver of the IPWP temperature as observed in temperature records globally (Shakun et al., 2012).

All but two of the existing SST records from the IPWP show warming coincident with or after the deglacial increase in CO_2, in support of the timing we infer from Lake Towuti (Figure 8). However, the wide range of timing of deglacial warming in IPWP SST records remains difficult to explain and does not exhibit clear patterns that might relate to ocean circulation. SST records from the Makassar Strait (SO217-18519) and the Timor Sea (MD01-2378) show deglacial warming began prior to increasing atmospheric CO_2 concentrations (Schröder et al., 2018; Xu et al., 2008; Figure 8), as does warming in the Sulu Sea record (MD97-2141) as described in the original publication (Rosenthal et al., 2003). Our method does not indicate deglacial warming in the Sulu Sea record until ~16.5 ka, but may be sensitive to the hiatus in sedimentation from 27.2 to 21.8 ka. Warming was reported to begin at 20 ka by Rosenthal et al. (2003).

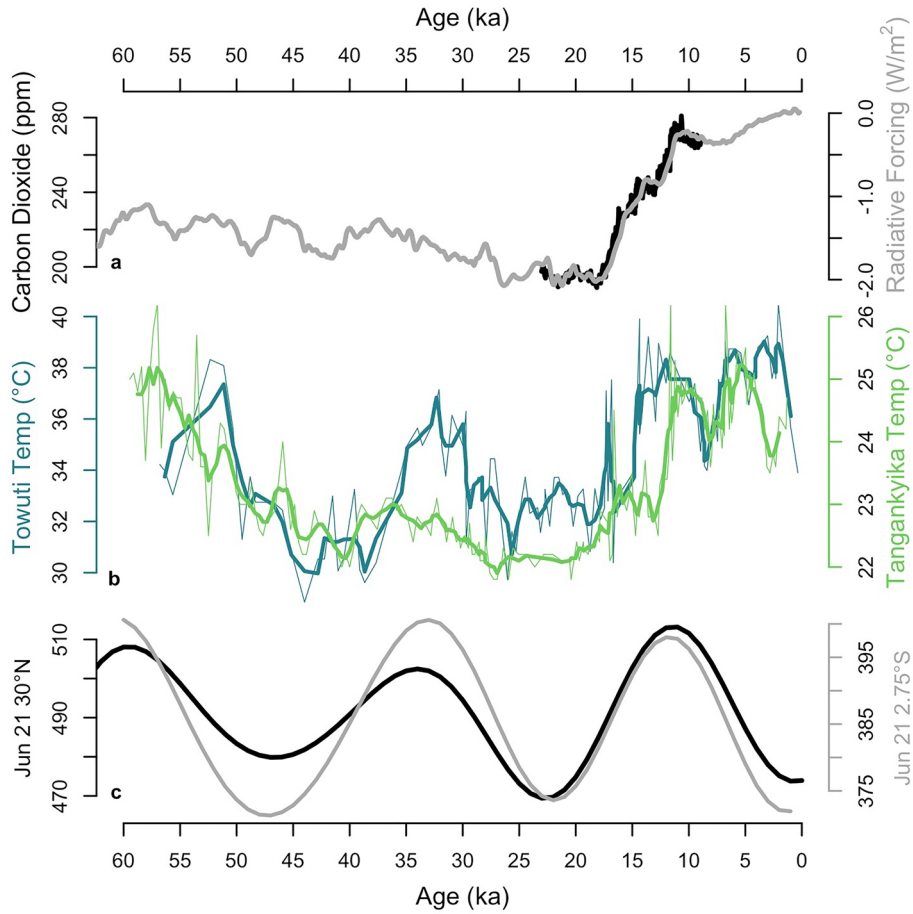

Figure 9. (a) Atmospheric CO_2 concentrations (black; Marcott et al., 2014), and radiative forcing of atmospheric carbon dioxide (gray; Schilt et al., 2010). (b) The reconstructed temperature from Lake Towuti (teal; this study) and the reconstructed lake surface temperature from Lake Tanganyika (green; Tierney et al., 2008), both plotted with a 1,500-year moving average. (c) June 21 insolation from 30°S (black; Berger & Loutre, 1991) and June 21 insolation from 2.75°S (gray; Laskar et al., 2004).

Exposure of the Sunda and Sahul Shelves is often invoked to explain deglacial changes in hydroclimate proxies from the LGM to modern in the IPWP (DiNezio et al., 2016, 2018; DiNezio & Tierney, 2013; Griffiths et al., 2013; Windler et al., 2019, 2020), potentially due to changes in surface temperatures marked by cooling over exposed shelf areas. The flooding of the Sunda and Sahul Shelves began at 15.5 ka (Pico et al., 2020), lagging the onset of deglacial warming in the Lake Towuti and marine temperature reconstructions by ~2 kyr. The onset of warming before the inundation of the Maritime Continent shelves indicates that the flooding of the shelves did not cause warming on Sulawesi. These results do not necessarily contradict the hypothesis that shelf exposure affected regional precipitation patterns, as modeling studies suggest the cooling associated with shelf exposure is modest and largely restricted to exposed shelf areas (DiNezio et al., 2018).

The Lake Towuti temperature record shows considerable orbital-scale temperature variations in addition to the last deglaciation. Our MAAT reconstruction indicates peaks in temperature at 55, 34, and 11 ka, similar to the timing of peaks in both Northern Hemisphere summer insolation and local winter insolation (Figure 9b). Both summer insolation from 30°N and local (2.75°S) winter insolation exhibit peaks roughly around 58, 34, and 11 ka, and troughs around 47, 22, and 0 ka (Figure 9c). A temperature reconstruction from Lake Tanganyika in East Africa, located at 6.55°S, also shows peaks in temperature around the same time as summer insolation from 30°N (Tierney et al., 2008) and local winter insolation (Figure 9b). A correlation between temperature and local winter insolation could imply a seasonal bias in our temperature reconstruction likely due to excess winter production of brGDGTs. Excess winter production of brGDGTs is plausible because winter is the mixing season and flux studies suggest increase brGDGT productions after lake mixing seasons (van Bree et al., 2020).

However, due to the lack of seasonality near the equator, we suggest that it is more likely that temperature at Lake Towuti is related to Northern Hemisphere summer insolation due to the influence of Northern Hemisphere insolation on the tropical monsoon (Guo et al., 2012; Ruddiman, 2003; Ruddiman & Raymo, 2003). Feedbacks between temperature and the hydrological cycle have been shown to be important in tropical Africa on orbital timescales (Dee et al., 2021; Gasse, 2000). The covariance between Northern Hemisphere insolation and temperature at Lake Towuti appears to break down during the Holocene, similar to the observation that methane from the Greenland Vostok ice cores diverges from Northern Hemisphere summer insolation at ∼5 ka that has been attributed to forest clearance and rice cultivation (Ruddiman, 2003). The breakdown of the covariance between temperature and Northern Hemisphere summer insolation when greenhouse gas concentrations are high further highlights the importance of greenhouse gas concentrations for controlling IPWP climate.

5. Conclusions

The onset of deglacial warming at 17.5 ka indicated in the Lake Towuti temperature reconstruction provides support for CO_2 as the primary mechanism forcing IPWP temperature from the LGM to modern. Northern Hemisphere summer insolation also appears to influence temperature in the IPWP and southeast Africa. The primary control of greenhouse gas concentrations on temperature in the IPWP raises concerns that greenhouse gas-forced climate changes in the IPWP could pose a threat to a region already experiencing frequent floods and landslides that are attributed to anthropogenic climate change.

Data Availability Statement

The radiocarbon ages, fractional abundances of brGDGTs, and the temperature reconstruction are available in the PANGEA data repository (Parish, 2022).

Acknowledgments
This material is based on work supported by National Science Foundation Grant EAR-2102856. The authors thank Gerald Tamuntuan, Satrio Wicaksono, Nigel Wattrus, and PT Vale Indonesia for field assistance. The authors acknowledge assistance and permission for this work from the Indonesian Ministry of Research and Technology (RISTEK). The authors also thank two anonymous reviewers for their thoughtful comments.

References

Baxter, A. J., van Bree, L. G. J., Peterse, F., Hopmans, E. C., Villanueva, L., Verschuren, D., & Sinninghe Damsté, J. S. (2021). Seasonal and multi-annual variation in the abundance of isoprenoid GDGT membrane lipids and their producers in the water column of a meromictic equatorial crater lake (Lake Chala, East Africa). *Quaternary Science Reviews*, *273*, 107263. https://doi.org/10.1016/j.quascirev.2021.107263

Berger, A., & Loutre, M. F. (1991). Insolation values for the climate of the last 10 million years. *Quaternary Science Reviews*, *10*(4), 297–317. https://doi.org/10.1016/0277-3791(91)90033-Q

Blaauw, M., & Christen, J. A. (2011). Flexible paleoclimate age-depth models using an autoregressive gamma process. *Bayesian Analysis*, *6*(3), 457–474. https://doi.org/10.1214/11-BA618

Bolliet, T., Holbourn, A., Kuhnt, W., Laj, C., Kissel, C., Beaufort, L., et al. (2011). Mindanao Dome variability over the last 160 kyr: Episodic glacial cooling of the West Pacific warm pool. *Paleoceanography*, *26*(1), PA1208. https://doi.org/10.1029/2010PA001966

Chiang, J. C. H. (2009). The tropics in paleoclimate. *Annual Review of Earth and Planetary Sciences*, *37*(1), 263–297. https://doi.org/10.1146/annurev.earth.031208.100217

Clement, A. C., Hall, A., & Broccoli, A. J. (2004). The importance of precessional signals in the tropical climate. *Climate Dynamics*, *22*(4), 327–341. https://doi.org/10.1007/s00382-003-0375-8

Costa, K. M., Russell, J. M., Vogel, H., & Bijaksana, S. (2015). Hydrological connectivity and mixing of Lake Towuti, Indonesia in response to paleoclimatic changes over the last 60,000 years. *Palaeogeography, Palaeoclimatology, Palaeoecology*, *417*, 467–475. https://doi.org/10.1016/j.palaeo.2014.10.009

Crowe, S. A., O'Neill, A. H., Katsev, S., Hehanussa, P., Haffner, G. D., Sundby, B., et al. (2008). The biogeochemistry of tropical lakes: A case study from Lake Matano, Indonesia. *Limnology & Oceanography*, *53*(1), 319–331. https://doi.org/10.4319/lo.2008.53.1.0319

Current Population. (2022). Current population. Retrieved from https://www.census.gov/popclock/print.php?component=counter

De Deckker, P. (2016). The Indo-Pacific warm pool: Critical to world oceanography and world climate. *Geoscience Letters*, 3(1), 20. https://doi.org/10.1186/s40562-016-0054-3

Dee, S. G., Morrill, C., Kim, S. H., & Russell, J. M. (2021). Hot air, hot lakes, or both? Exploring mid-holocene african temperatures using proxy system modeling. *Journal of Geophysical Research: Atmospheres*, *126*(10), e2020JD033269. https://doi.org/10.1029/2020JD033269

De Jonge, C., Hopmans, E. C., Stadnitskaia, A., Rijpstra, W. I. C., Hofland, R., Tegelaar, E., & Sinninghe Damsté, J. S. (2013). Identification of novel penta- and hexamethylated branched glycerol dialkyl glycerol tetraethers in peat using HPLC–MS2, GC–MS and GC–SMB-MS. *Organic Geochemistry*, *54*, 78–82. https://doi.org/10.1016/j.orggeochem.2012.10.004

De Jonge, C., Hopmans, E. C., Zell, C. I., Kim, J.-H., Schouten, S., & Sinninghe Damsté, J. S. (2014). Occurrence and abundance of 6-methyl branched glycerol dialkyl glycerol tetraethers in soils: Implications for palaeoclimate reconstruction. *Geochimica et Cosmochimica Acta*, *141*, 97–112. https://doi.org/10.1016/j.gca.2014.06.013

DiNezio, P. N., & Tierney, J. E. (2013). The effect of sea level on glacial Indo-Pacific climate. *Nature Geoscience*, *6*(6), 485–491. https://doi.org/10.1038/ngeo1823

DiNezio, P. N., Tierney, J. E., Otto-Bliesner, B. L., Timmermann, A., Bhattacharya, T., Rosenbloom, N., & Brady, E. (2018). Glacial changes in tropical climate amplified by the Indian Ocean. *Science Advances*, *4*(12), eaat9658. https://doi.org/10.1126/sciadv.aat9658

DiNezio, P. N., Timmermann, A., Tierney, J. E., Jin, F.-F., Otto-Bliesner, B., Rosenbloom, N., et al. (2016). The climate response of the Indo-Pacific warm pool to glacial sea level. *Paleoceanography*, *31*(6), 866–894. https://doi.org/10.1002/2015PA002890

Fan, W., Jian, Z., Chu, Z., Dang, H., Wang, Y., Bassinot, F., et al. (2018). Variability of the Indonesian throughflow in the Makassar Strait over the last 30 ka. *Scientific Reports*, *8*(1), 5678. https://doi.org/10.1038/s41598-018-24055-1

Gasse, F. (2000). Hydrological changes in the African tropics since the last glacial maximum. *Quaternary Science Reviews*, *19*(1), 189–211. https://doi.org/10.1016/S0277-3791(99)00061-X

Gibbons, F. T., Oppo, D. W., Mohtadi, M., Rosenthal, Y., Cheng, J., Liu, Z., & Linsley, B. K. (2014). Deglacial δ18O and hydrologic variability in the tropical Pacific and Indian Oceans. *Earth and Planetary Science Letters*, *387*, 240–251. https://doi.org/10.1016/j.epsl.2013.11.032

Griffiths, M. L., Drysdale, R. N., Gagan, M. K., Zhao, J., Hellstrom, J. C., Ayliffe, L. K., & Hantoro, W. S. (2013). Abrupt increase in east Indonesian rainfall from flooding of the Sunda Shelf ~9500 years ago. *Quaternary Science Reviews*, *74*, 273–279. https://doi.org/10.1016/j.quascirev.2012.07.006

Guo, Z., Zhou, X., & Wu, H. (2012). Glacial-interglacial water cycle, global monsoon and atmospheric methane changes. *Climate Dynamics*, *39*(5), 1073–1092. https://doi.org/10.1007/s00382-011-1147-5

Hamilton, N. (2022). ggtern: An extension to "ggplot2", for the creation of ternary diagrams (version 3.4.1). Retrieved from https://CRAN.R-project.org/package=ggtern

Hijmans, R. J., Etten, J. V., Sumner, M., Cheng, J., Baston, D., Bevan, A., et al. (2022). raster: Geographic data analysis and modeling (version 3.5-15). Retrieved from https://CRAN.R-project.org/package=raster

Holbourn, A., Kuhnt, W., & Xu, J. (2011). Indonesian Throughflow variability during the last 140 ka: The Timor Sea outflow. *Geological Society, London, Special Publications*, *355*(1), 283–303. https://doi.org/10.1144/SP355.14

Hope, G. (2001). Environmental change in the late Pleistocene and later Holocene at Wanda site, Soroako, South Sulawesi, Indonesia. *Palaeogeography, Palaeoclimatology, Palaeoecology*, *171*(3), 129–145. https://doi.org/10.1016/S0031-0182(01)00243-7

Hopmans, E. C., Schouten, S., & Sinninghe Damsté, J. S. (2016). The effect of improved chromatography on GDGT-based palaeoproxies. *Organic Geochemistry*, *93*, 1–6. https://doi.org/10.1016/j.orggeochem.2015.12.006

Hopmans, E. C., Weijers, J. W. H., Schefuß, E., Herfort, L., Sinninghe Damsté, J. S., & Schouten, S. (2004). A novel proxy for terrestrial organic matter in sediments based on branched and isoprenoid tetraether lipids. *Earth and Planetary Science Letters*, *224*(1), 107–116. https://doi.org/10.1016/j.epsl.2004.05.012

Jian, Z., Wang, Y., Dang, H., Lea, D. W., Liu, Z., Jin, H., & Yin, Y. (2020). Half-precessional cycle of thermocline temperature in the Western equatorial Pacific and its bihemispheric dynamics. *Proceedings of the National Academy of Sciences*, *117*(13), 7044–7051. https://doi.org/10.1073/pnas.1915510117

Juggins, S. (2022). rioja: Analysis of quaternary science data (version 1.0-5). Retrieved from https://CRAN.R-project.org/package=rioja

Kalnay, E., Kanamitsu, M., Kistler, R., Collins, W., Deaven, D., Gandin, L., et al. (1996). The NCEP/NCAR 40-year reanalysis project. *Bulletin of the American Meteorological Society*, *77*(3), 437–472. https://doi.org/10.1175/1520-0477(1996)077<0437:TNYRP>2.0.CO;2

Killick, R., Beaulieu, C., Taylor, S., & Hullait, H. (2021). EnvCpt: Detection of structural changes in climate and environment time series (version 1.1.3). Retrieved from https://CRAN.R-project.org/package=EnvCpt

Konecky, B., Russell, J., & Bijaksana, S. (2016). Glacial aridity in central Indonesia coeval with intensified monsoon circulation. *Earth and Planetary Science Letters*, *437*, 15–24. https://doi.org/10.1016/j.epsl.2015.12.037

Laskar, J., Robutel, P., Joutel, F., Gastineau, M., Correia, A. C. M., & Levrard, B. (2004). A long-term numerical solution for the insolation quantities of the Earth. *Astronomy & Astrophysics*, *428*(1), 261–285. https://doi.org/10.1051/0004-6361:20041335

Levi, C., Labeyrie, L., Bassinot, F., Guichard, F., Cortijo, E., Waelbroeck, C., et al. (2007). Low-latitude hydrological cycle and rapid climate changes during the last deglaciation. *Geochemistry, Geophysics, Geosystems*, *8*(5). https://doi.org/10.1029/2006GC001514

Loomis, S. E., Russell, J. M., Eggermont, H., Verschuren, D., & Sinninghe Damsté, J. S. (2014). Effects of temperature, pH and nutrient concentration on branched GDGT distributions in East African lakes: Implications for paleoenvironmental reconstruction. *Organic Geochemistry*, *66*, 25–37. https://doi.org/10.1016/j.orggeochem.2013.10.012

Loomis, S. E., Russell, J. M., Ladd, B., Street-Perrott, F. A., & Sinninghe Damsté, J. S. (2012). Calibration and application of the branched GDGT temperature proxy on East African lake sediments. *Earth and Planetary Science Letters*, *357*(358), 277–288. https://doi.org/10.1016/j.epsl.2012.09.031

Marcott, S. A., Bauska, T. K., Buizert, C., Steig, E. J., Rosen, J. L., Cuffey, K. M., et al. (2014). Centennial-scale changes in the global carbon cycle during the last deglaciation. *Nature*, *514*(7524), 616–619. https://doi.org/10.1038/nature13799

Martínez-Sosa, P., & Tierney, J. E. (2019). Lacustrine brGDGT response to microcosm and mesocosm incubations. *Organic Geochemistry*, *127*, 12–22. https://doi.org/10.1016/j.orggeochem.2018.10.011

Martínez-Sosa, P., Tierney, J. E., Stefanescu, I. C., Dearing Crampton-Flood, E., Shuman, B. N., & Routson, C. (2021). A global Bayesian temperature calibration for lacustrine brGDGTs. *Geochimica et Cosmochimica Acta*, *305*, 87–105. https://doi.org/10.1016/j.gca.2021.04.038

Mohtadi, M., Prange, M., Oppo, D. W., De Pol-Holz, R., Merkel, U., Zhang, X., et al. (2014). North Atlantic forcing of tropical Indian Ocean climate. *Nature*, *509*(7498), 76–80. https://doi.org/10.1038/nature13196

Naafs, B. D. A., Oliveira, A. S. F., & Mulholland, A. J. (2021). Molecular dynamics simulations support the hypothesis that the brGDGT paleothermometer is based on homeoviscous adaptation. *Geochimica et Cosmochimica Acta*, *312*, 44–56. https://doi.org/10.1016/j.gca.2021.07.034

Oksanen, J., Blanchet, F. G., Friendly, M., Kindt, R., Legendre, P., McGlinn, D., et al. (2020). vegan: Community ecology package. Retrieved from https://CRAN.R-project.org/package=vegan

Parish, M. C. (2022). A brGDGT-based reconstruction of terrestrial temperature from the Maritime Continent spanning the Last Glacial Maximum [Dataset]. PANGAEA. https://doi.org/10.1594/PANGAEA.948194

Pico, T., McGee, D., Russell, J., & Mitrovica, J. X. (2020). Recent constraints on MIS 3 sea level support role of continental shelf exposure as a control on Indo-Pacific hydroclimate. *Paleoceanography and Paleoclimatology*, *35*(8). https://doi.org/10.1029/2020PA003998

Powers, L., Werne, J. P., Vanderwoude, A. J., Sinninghe Damsté, J. S., Hopmans, E. C., & Schouten, S. (2010). Applicability and calibration of the TEX86 paleothermometer in lakes. *Organic Geochemistry*, *41*(4), 404–413. https://doi.org/10.1016/j.orggeochem.2009.11.009

Raberg, J. H., Harning, D. J., Crump, S. E., de Wet, G., Blumm, A., Kopf, S., et al. (2021). Revised fractional abundances and warm-season temperatures substantially improve brGDGT calibrations in lake sediments. *Biogeosciences Discussions*, 1–36. https://doi.org/10.5194/bg-2021-16

Reeves, J. M., Bostock, H. C., Ayliffe, L. K., Barrows, T. T., De Deckker, P., Devriendt, L. S., et al. (2013). Palaeoenvironmental change in tropical Australasia over the last 30,000 years – A synthesis by the OZ-INTIMATE group. *Quaternary Science Reviews*, *74*, 97–114. https://doi.org/10.1016/j.quascirev.2012.11.027

Rosenthal, Y., Oppo, D. W., & Linsley, B. K. (2003). The amplitude and phasing of climate change during the last deglaciation in the Sulu Sea, Western equatorial Pacific: The amplitude and phasing of climate change. *Geophysical Research Letters*, *30*(8). https://doi.org/10.1029/2002GL016612

Ruddiman, W. F. (2003). The anthropogenic greenhouse era began thousands of years ago. *Climatic Change*, *61*(3), 261–293. https://doi.org/10.1023/B:CLIM.0000004577.17928.fa

Ruddiman, W. F., & Raymo, M. E. (2003). A methane-based time scale for Vostok ice. *Quaternary Science Reviews*, *22*(2), 141–155. https://doi.org/10.1016/S0277-3791(02)00082-3

Russell, J. M., Hopmans, E. C., Loomis, S. E., Liang, J., & Sinninghe Damsté, J. S. (2018). Distributions of 5- and 6-methyl branched glycerol dialkyl glycerol tetraethers (brGDGTs) in East African lake sediment: Effects of temperature, pH, and new lacustrine paleotemperature calibrations. *Organic Geochemistry*, *117*, 56–69. https://doi.org/10.1016/j.orggeochem.2017.12.003

Russell, J. M., Vogel, H., Bijaksana, S., Melles, M., Deino, A., Hafidz, A., et al. (2020). The late quaternary tectonic, biogeochemical, and environmental evolution of ferruginous Lake Towuti, Indonesia. *Palaeogeography, Palaeoclimatology, Palaeoecology*, *556*, 109905. https://doi.org/10.1016/j.palaeo.2020.109905

Russell, J. M., Vogel, H., Konecky, B. L., Bijaksana, S., Huang, Y., Melles, M., et al. (2014). Glacial forcing of central Indonesian hydroclimate since 60,000 y B.P. *Proceedings of the National Academy of Sciences*, *111*(14), 5100–5105. https://doi.org/10.1073/pnas.1402373111

Schilt, A., Baumgartner, M., Schwander, J., Buiron, D., Capron, E., Chappellaz, J., et al. (2010). Atmospheric nitrous oxide during the last 140,000years. *Earth and Planetary Science Letters*, *300*(1), 33–43. https://doi.org/10.1016/j.epsl.2010.09.027

Schouten, S., Hopmans, E. C., Schefuß, E., & Sinninghe Damsté, J. S. (2002). Distributional variations in marine crenarchaeotal membrane lipids: A new tool for reconstructing ancient sea water temperatures? *Earth and Planetary Science Letters*, *204*(1), 265–274. https://doi.org/10.1016/S0012-821X(02)00979-2

Schröder, J. F., Kuhnt, W., Holbourn, A., Beil, S., Zhang, P., Hendrizan, M., & Xu, J. (2018). Deglacial warming and hydroclimate variability in the central Indonesian archipelago. *Paleoceanography and Paleoclimatology*, *33*(9), 974–993. https://doi.org/10.1029/2018PA003323

Setiawan, R. Y., Mohtadi, M., Southon, J., Groeneveld, J., Steinke, S., & Hebbeln, D. (2015). The consequences of opening the Sunda Strait on the hydrography of the eastern tropical Indian Ocean. *Paleoceanography*, *30*(10), 1358–1372. https://doi.org/10.1002/2015PA002802

Shakun, J. D., Clark, P. U., He, F., Marcott, S. A., Mix, A. C., Liu, Z., et al. (2012). Global warming preceded by increasing carbon dioxide concentrations during the last deglaciation. *Nature*, *484*(7392), 49–54. https://doi.org/10.1038/nature10915

Sinninghe Damsté, J. S., Ossebaar, J., Schouten, S., & Verschuren, D. (2012). Distribution of tetraether lipids in the 25-ka sedimentary record of Lake Challa: Extracting reliable TEX86 and MBT/CBT palaeotemperatures from an equatorial African lake. *Quaternary Science Reviews*, *50*, 43–54. https://doi.org/10.1016/j.quascirev.2012.07.001

Stefanescu, I. C., Shuman, B. N., & Tierney, J. E. (2021). Temperature and water depth effects on brGDGT distributions in sub-alpine lakes of mid-latitude North America. *Organic Geochemistry*, *152*, 104174. https://doi.org/10.1016/j.orggeochem.2020.104174

Steinke, S., Chiu, H.-Y., Yu, P.-S., Shen, C.-C., Erlenkeuser, H., Löwemark, L., & Chen, M.-T. (2006). On the influence of sea level and monsoon climate on the southern South China Sea freshwater budget over the last 22,000 years. *Quaternary Science Reviews*, *25*(13), 1475–1488. https://doi.org/10.1016/j.quascirev.2005.12.008

Stott, L., Timmermann, A., & Thunell, R. (2007). Southern hemisphere and deep-sea warming led deglacial atmospheric CO_2 rise and tropical warming. *Science*, *318*(5849), 435–438. https://doi.org/10.1126/science.1143791

Tierney, J. E., & Russell, J. M. (2009). Distributions of branched GDGTs in a tropical lake system: Implications for lacustrine application of the MBT/CBT paleoproxy. *Organic Geochemistry*, *40*(9), 1032–1036. https://doi.org/10.1016/j.orggeochem.2009.04.014

Tierney, J. E., Russell, J. M., Eggermont, H., Hopmans, E. C., Verschuren, D., & Sinninghe Damsté, J. S. (2010). Environmental controls on branched tetraether lipid distributions in tropical East African lake sediments. *Geochimica et Cosmochimica Acta*, *74*(17), 4902–4918. https://doi.org/10.1016/j.gca.2010.06.002

Tierney, J. E., Russell, J. M., Huang, Y., Damsté, J. S. S., Hopmans, E. C., & Cohen, A. S. (2008). Northern hemisphere controls on tropical southeast African climate during the past 60,000 years. *Science*, *322*(5899), 252–255. https://doi.org/10.1126/science.1160485

Tierney, J. E., Schouten, S., Pitcher, A., Hopmans, E. C., & Sinninghe Damsté, J. S. (2012). Core and intact polar glycerol dialkyl glycerol tetraethers (GDGTs) in Sand Pond, Warwick, Rhode Island (USA): Insights into the origin of lacustrine GDGTs. *Geochimica et Cosmochimica Acta*, *77*, 561–581. https://doi.org/10.1016/j.gca.2011.10.018

van Bree, L. G. J., Peterse, F., Baxter, A. J., De Crop, W., van Grinsven, S., Villanueva, L., et al. (2020). Seasonal variability and sources of in situ brGDGT production in a permanently stratified African crater lake. *Biogeosciences*, *17*(21), 5443–5463. https://doi.org/10.5194/bg-17-5443-2020

Vuillemin, A., Friese, A., Alawi, M., Henny, C., Nomosatryo, S., Wagner, D., et al. (2016). Geomicrobiological features of ferruginous sediments from Lake Towuti, Indonesia. *Frontiers in Microbiology*, *7*. https://doi.org/10.3389/fmicb.2016.01007

Wang, X., Jian, Z., Lückge, A., Wang, Y., Dang, H., & Mohtadi, M. (2018). Precession-paced thermocline water temperature changes in response to upwelling conditions off southern Sumatra over the past 300,000 years. *Quaternary Science Reviews*, *192*, 123–134. https://doi.org/10.1016/j.quascirev.2018.05.035

Wei, T., Simko, V., Levy, M., Xie, Y., Jin, Y., Zemla, J., et al. (2021). corrplot: Visualization of a correlation matrix (version 0.92). Retrieved from https://CRAN.R-project.org/package=corrplot

Weijers, J. W. H., Schouten, S., van den Donker, J. C., Hopmans, E. C., & Sinninghe Damsté, J. S. (2007). Environmental controls on bacterial tetraether membrane lipid distribution in soils. *Geochimica et Cosmochimica Acta*, *71*(3), 703–713. https://doi.org/10.1016/j.gca.2006.10.003

Windler, G., Tierney, J. E., DiNezio, P. N., Gibson, K., & Thunell, R. (2019). Shelf exposure influence on Indo-Pacific Warm Pool climate for the last 450,000 years. *Earth and Planetary Science Letters*, *516*, 66–76. https://doi.org/10.1016/j.epsl.2019.03.038

Windler, G., Tierney, J. E., Zhu, J., & Poulsen, C. J. (2020). Unraveling glacial hydroclimate in the Indo-Pacific warm pool: Perspectives from water isotopes. *Paleoceanography and Paleoclimatology*, *35*(12), e2020PA003985. https://doi.org/10.1029/2020PA003985

Wu, J., Yang, H., Pancost, R. D., Naafs, B. D. A., Qian, S., Dang, X., et al. (2021). Variations in dissolved O_2 in a Chinese lake drive changes in microbial communities and impact sedimentary GDGT distributions. *Chemical Geology*, *579*, 120348. https://doi.org/10.1016/j.chemgeo.2021.120348

Xu, J., Holbourn, A., Kuhnt, W., Jian, Z., & Kawamura, H. (2008). Changes in the thermocline structure of the Indonesian outflow during Terminations I and II. *Earth and Planetary Science Letters*, *273*(1), 152–162. https://doi.org/10.1016/j.epsl.2008.06.029

Yao, Y., Zhao, J., Vachula, R. S., Werne, J. P., Wu, J., Song, X., & Huang, Y. (2020). Correlation between the ratio of 5-methyl hexamethylated to pentamethylated branched GDGTs (HP5) and water depth reflects redox variations in stratified lakes. *Organic Geochemistry*, *147*, 104076. https://doi.org/10.1016/j.orggeochem.2020.104076